ACS APPLIED MATERIALS & INTERFACES

Research Article

www.acsami.org

Modulating the Morphology and Electrical Properties of GaAs Nanowires via Catalyst Stabilization by Oxygen

Ning Han,[†,‡,§] Zaixing Yang,[‡,⊥,§] Fengyun Wang,[∥] SenPo Yip,[‡,⊥] Guofa Dong,[‡] Xiaoguang Liang,[‡] TakFu Hung,[‡] Yunfa Chen,[†] and Johnny C. Ho*[,‡,⊥]

[†]State Key Laboratory of Multiphase Complex Systems, Institute of Process Engineering, Chinese Academy of Sciences, Beijing 100190, P. R. China

[‡]Department of Physics and Materials Science, City University of Hong Kong, Hong Kong SAR, P. R. China

[⊥]Shenzhen Research Institute, City University of Hong Kong, Shenzhen 518057, P. R. China

[∥]Cultivation Base for State Key Laboratory, Qingdao University, Qingdao 266071, P. R. China

Supporting Information

ABSTRACT: Nowadays, III−V compound semiconductor nanowires (NWs) have attracted extensive research interest because of their high carrier mobility favorable for next-generation electronics. However, it is still a great challenge for the large-scale synthesis of III−V NWs with well-controlled and uniform morphology as well as reliable electrical properties, especially on the low-cost noncrystalline substrates for practical utilization. In this study, high-density GaAs NWs with lengths >10 μm and uniform diameter distribution (relative standard deviation $\sigma \sim 20\%$) have been successfully prepared by annealing the Au catalyst films (4−12 nm) in air right before GaAs NW growth, which is in distinct contrast to the ones of 2−3 μm length and widely distributed of $\sigma \sim 20$−60% of the conventional NWs grown by the H_2-annealed film. This air-annealing process is found to stabilize the Au nanoparticle seeds and to minimize Ostwald ripening during NW growth. Importantly, the obtained GaAs NWs exhibit uniform p-type conductivity when fabricated into NW-arrayed thin-film field-effect transistors (FETs). Moreover, they can be integrated with an n-type InP NW FET into effective complementary metal oxide semiconductor inverters, capable of working at low voltages of 0.5−1.5 V. All of these results explicitly demonstrate the promise of these NW morphology and electrical property controls through the catalyst engineering for next-generation electronics.

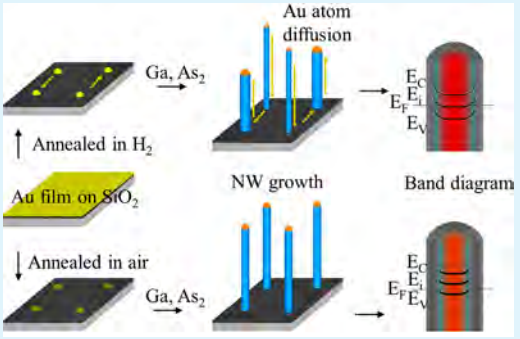

KEYWORDS: *GaAs nanowire, oxygen, diameter control, electronic property, CMOS inverter*

INTRODUCTION

In recent years, because of the excellent physical and electrical properties, high-carrier-mobility III−V semiconductor nanowire (NW) materials such as GaAs, InAs, GaSb, and InSb are widely investigated for next-generation electronics and optics.[1−9] Particularly, GaAs and InAs NWs with electron mobility in the order of 10^3−10^4 $cm^2/(Vs)$ are readily obtained using chemical vapor deposition (CVD) via vapor−liquid−solid (VLS) and/or vapor−solid−solid (VSS) growth mechanisms,[4,10] which are promising for applications in the complementary metal−oxide−semiconductor (CMOS) technology beyond the silicon era.[2,11,12] At the same time, for most practical utilizations, the large-scale preparation of NWs with uniform diameter is highly desirable because the corresponding electrical and optical properties are found to be heavily dependent on the NW dimensions. For example, the electron mobility of most III−V NWs is determined to decrease with diameter reduction,[4,13,14] while band-gap luminescence is observed to blue-shift with a decrease of the GaAs NW thickness.[15,16] Other factors influencing the NW electrical and optical properties including the phase transition, preferential crystal orientation, and defect density are also proven to be closely related with the NW diameter.[13,17−19] Nevertheless, most of the NWs prepared in CVD involving the metal−organic source (i.e., MOCVD) or solid source (i.e., SSCVD) have a relatively large diameter distribution because of the greatly varied diameters of the metal catalytic seeds, which would lead to the varied and uncontrolled NW properties.[5,20−22]

In general, III−V NWs prepared by catalytic metal seeds annealed from thin metal films (e.g., 0.1−2 nm) have narrower diameter distributions with relative standard deviations of $\sigma \sim$ 20−30%,[20,21,23] while those from thick metal films (e.g., 4−20 nm) have far larger diameter distributions (e.g., $\sigma > 50\%$).[20] On the other hand, even though metal nanocolloidals prepared in the liquid phase can have relatively uniform diameters ($\sigma \sim 5$−

Received: January 22, 2015
Accepted: February 20, 2015
Published: February 20, 2015

DOI: 10.1021/acsami.5b00666
ACS Appl. Mater. Interfaces 2015, 7, 5591−5597

10%) by fine-tuning synthesis conditions and well-chosen surfactants,[24,25] the resultant NWs might still have large diameter distributions because the colloidal seeds would also suffer from high-temperature Ostwald ripening and even merging to form larger catalytic clusters during the growth process,[26−29] unavoidably leading to the nonuniformity of corresponding NW diameters as well as their electrical properties. In this regard, Wu et al. adopted the porous alumina oxide as the template to deposit uniform Au clusters for the growth of GaAs NWs with uniform diameters.[22] Although this complex growth process is effective in reducing the NW diameter distribution, the obtained σ is still larger than 10% with a relatively short growth time of ∼30 min and a NW length of ∼135 nm (i.e., more like nanorods), where the Ostwald ripening and merging effect is minimized. As a result, a simple, effective, and reliable catalyst engineering technique is essential for the large-scale fabrication of VLS and/or VSS NWs with controllable diameter, uniform morphology, and physical properties, especially for those grown on noncrystalline substrates for cost minimization.

Lately, by utilizing in situ transmission electron microscopy (TEM), Kodambaka et al. found that a trace amount of oxygen existed in the CVD system would retard Ostwald ripening of Au catalytic particles for Si NW growth through stabilization of Au atoms, and thus no NW tapering is observed.[27] In addition to the widely adopted Au catalysts, oxidizing Cu nanoparticles into oxide is essential for the efficient CVD synthesis of Si NWs.[30] Even if no corresponding electrical or optical property of obtained NWs is measured, all of these findings would certainly infer the importance of catalyst stabilization by oxygen for the growth of Si NWs, which was however still lacking in III−V NW growth until now. In this study, we adopted thick Au catalyst films with nominal thicknesses of 4−12 nm for the CVD growth of GaAs NWs and found that the NWs would have a rather uniform diameter distribution ($\sigma \sim 20\%$) by just stabilizing (i.e., annealing) the Au film in ambient air before growth compared with the one annealed in the H_2 environment ($\sigma \sim 20-60\%$) for conventional NW growth. Moreover, these uniform, long, and dense NWs obtained through oxygen stabilization of the Au catalyst can further enable the high-density NW-parallel-arrayed integration achieved by contact printing, demonstrating the uniform p-type characteristic that is in distinct contrast with their ambipolar counterparts grown without catalyst stabilization. Then, the p-type GaAs NW-parallel-arrayed thin-film field-effect transistor (FET) is subsequently integrated with the n-type InP NW FET to attain CMOS inverters capable of operating at a voltage as low as 0.5 V, illustrating the promise of NW synthesis by simply engineering the catalyst for large-scale applications in next-generation electronics.

EXPERIMENTAL SECTION

GaAs NW Synthesis and Characterization. The GaAs NWs are synthesized in a solid-source CVD system using the Au catalyst film as reported previously.[18,31] In detail, the boron nitride crucible holding GaAs powders (∼1 g, 99.9999% purity) and the SiO_2/Si substrate wafer (50-nm-thick thermal oxide) with Au thin films (4−12 nm) thermally predeposited are placed in the upstream and downstream zones of a two-zone tube furnace, respectively, serving as the solid source and the growth catalyst. After the system is pumped down to $\sim 10^{-3}$ Torr, H_2 gas (100 standard cm^3/min or sccm, 99.999% purity) is provided through control of the mass flow controller and the Au catalyst film is annealed into nanoparticles at 800 °C for 10 min. After the catalyst zone is cooled to the growth temperature (600 °C), the upstream zone starts to ramp up to 820 °C to evaporate the GaAs powders, and the vapor precursors are then transported by H_2 to the downstream zone for NW growth. After a duration of 60 min, the system is cooled to room temperature in a H_2 atmosphere, and next the NWs are harvested for subsequent characterization and device fabrication. The only difference of the growth method performed in this study is that the Au catalyst film is first annealed in air at 800 °C for 10 min, and at that moment the system is pumped down to $\sim 10^{-3}$ Torr for NW growth in the same H_2 atmosphere with the same growth details.

The morphology of GaAs NWs is observed by scanning electron microscopy (SEM; FEI/Philips XL30, Philips Electronics, Amsterdam, The Netherlands) and transmission electron microscopy (TEM; Philips CM20). X-ray diffraction (XRD) is recorded on a Philips powder diffractometer (40 kV, 30 mA) using Cu Kα radiation (λ = 0.154 nm). Energy-dispersive X-ray spectroscopy (EDS) spectra and selective area electron diffraction (SAED) patterns are obtained by TEM (Philips CM20). Also, surface elemental analysis is carried out by X-ray photoelectron spectroscopy (XPS; model 5802, ULVAC-PHI Inc., Kanagawa, Japan).

Device Fabrication and Measurement. The GaAs NW-parallel-arrayed FET is fabricated by contact printing as reported previously.[32] Specifically, a device substrate SiO_2/Si (50 nm thick and thermally grown) is patterned by photolithography (SUSS MA6), where the exposed area is modified by mild O_2 plasma and decorated with polylysine (0.5% v/v aqueous solution). Afterward, the GaAs NW donor substrate is moved into contact with the pattern at a velocity of 10 mm/min under a pressure of 50 g/cm^2, and the NW parallel array is attained after the lift-off of residual photoresist by sonication in acetone. The source/drain electrode pattern is next defined by photolithography, and Ni electrodes are deposited by thermal evaporation followed by the lift-off. The current−voltage ($I-V$) characteristics of the FET and the voltage transformation curves of the CMOS inverter are measured with an Agilent 4155C semiconductor analyzer in a standard probe station.

RESULTS AND DISCUSSION

The morphology and structural differences of GaAs NWs prepared by H_2 annealing and air stabilization of the Au catalyst are studied in detail by using a typical 6-nm-thick Au film. As shown in the SEM images in Figure 1a,b, GaAs NWs grown by the H_2-annealed Au film are relatively thick and short, with a length of only 2−3 μm. On the contrary, GaAs NWs prepared by the air-stabilized Au catalyst are thinner and longer (>10 μm). In order to identify the crystal structures, XRD patterns are obtained as depicted in Figure 1c, demonstrating that both NWs are grown in the standard zinc blende cubic phase (PDF 14-0450). This is further proven by the SAED pattern of an individual GaAs NW prepared by the air-stabilized Au film in Figure 1d, where a typical NW growth orientation of ⟨110⟩ is displayed. The TEM image (Figure 1d) also indicates clearly that a catalytic tip exists on top of the NW, comprised of Au and Ga analyzed by EDS, as shown in Figure S1 in the Supporting Information (SI), illustrating that the NWs are grown via the VLS and/or VSS mechanisms. These are in good agreement with the literature that the Ga precursors are generally diffused through the Au−Ga alloy seeds while the As component is incorporated through the interface from the gas phase.[18,33] On the basis of all of these observations, it is deduced that GaAs NWs prepared by the air-stabilized Au film are grown in the same structure via the same growth mechanism as those obtained by the H_2-annealed Au film. This is also in distinct contrast to those obtained by the oxide-assisted growth (OAG) method,[34,35] where no catalyst is used and thus the diameter is very unevenly distributed (e.g., 10−120 nm), while in this work, the Au catalytic particles are still

DOI: 10.1021/acsami.5b00666
ACS Appl. Mater. Interfaces 2015, 7, 5591−5597

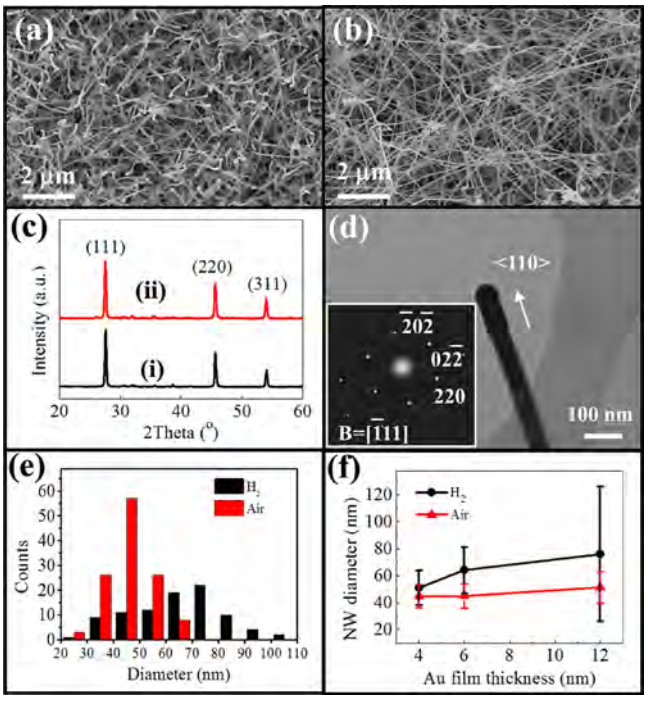

Figure 1. Comparison of GaAs NWs prepared by a 6-nm-thick Au catalyst film annealed in H_2 and in ambient air. (a and b) SEM images of GaAs NWs prepared by the H_2- and air-annealed Au catalyst films. (c) XRD patterns of (i) H_2-annealed and (ii) air-annealed GaAs NWs. (d) TEM and SAED pattern of an individual NW enabled by the air-stabilized catalyst. (e) Comparison of the NW diameter distribution obtained by the 6-nm-thick H_2- and air-annealed catalyst film, (f) comparison of the diameter statistics of GaAs NWs prepared by different thicknesses of Au films.

active for NW growth even after air stabilization because it is difficult to oxidize Au under these mild conditions; as a result, the NW diameter is dictated and determined by the Au catalytic tips here.[36] As given in Figure 1e, the NW diameter distribution is quantitatively compared by the statistics of ~100 NWs, in which a wide (64.1 ± 17.2 nm; $\sigma \sim 27\%$) and a narrow (45.1 ± 9.0 nm; $\sigma \sim 20\%$) diameter distribution are clearly seen for the GaAs NWs grown by H_2-annealed and air-stabilized Au catalyst films, respectively. Compared with GaAs NWs synthesized by other technologies (Table 1), it is clearly seen that this air-stabilization technique performed on the catalyst can significantly reduce the NW diameter distribution. Meanwhile, to further examine the effect of this air-stabilization effect, the Au film is also annealed in a vacuum (10^{-3} Torr) for GaAs NW growth. As shown in Figure S2 in the SI, the diameter of grown NWs is still distributed widely compared with the one obtained in the air-annealing process. Furthermore, the NW diameter statistics are also analyzed for different Au catalyst film thicknesses of 4–12 nm in Figure 1f, with the detailed corresponding SEM images and diameter histograms shown in Figure S3 in the SI. All of these results demonstrate obviously that the air-stabilized Au film would yield the much reduced NW diameter distribution, especially for the thick NWs with the same crystal structure and growth mechanism as those achieved with H_2-annealed films.

Table 1. Comparison of GaAs NW Diameter Distribution by Different Technologies in the Literature[a]

	catalyst	mechanism	diameter distribution (nm)	ref
SS-CVD	6 nm Au film	VLS	20–110	18
SS-CVD	6 nm Au film	VLS with oxygen	20–70	this study
MBE	3.3 nm Au film	VLS	10–70	20
	4.4 nm Au in AAO		20–50	
OAG	No	oxide-assisted	10–120	33
LCG	0.05% Au in target	VLS	3–30	8
SA-MOVPE	No	in holes of SiO_2 mask	50–100	9

[a]MBE: molecular beam epitaxy. LCG: laser-assisted catalytic growth. SA-MOVPE: selective area metal–organic vapor-phase epitaxy.

To shed light on how the air-stabilization step can affect the Au catalyst, the Au nanoparticle diameter distribution is compared in detail between the H_2-annealed and air-stabilized cases. First, the 6-nm-thick Au films annealed at 800 °C for 10 min in H_2 and in air both give the similar particle size, as is typically shown in the SEM image in Figure 2a, where Ostwald ripening is not significant in such a short time. However, after the annealing time is prolonged to 60 min, a significant difference of the particle size is observed, as illustrated in Figure 2b,c; that is, the Au nanoparticles annealed in H_2 become larger as intuitively observed, while the particles annealed in air keep similar sizes. The corresponding size distribution can be estimated by measuring 200 nanoparticles annealed for 60 min in H_2 and in air, as shown in Figure 2d. It is clear that the Au nanoparticle size distribution is wider (22.1 ± 7.8 nm; $\sigma \sim 35\%$) for the H_2-annealed sample than for the air-stabilized case (22.4 ± 5.4 nm; $\sigma \sim 24\%$), inferring that an Ostwald ripening process occurred for the Au nanoparticles annealed in H_2, which makes large particles grow larger at the expense of decreasing sizes of small particles. In order to correlate the deposited nominal Au film thickness and the obtained Au nanoparticle dimension after annealing, it can be estimated that the equivalent Au film thickness is ~5.3 nm based on the diameter histogram and the nanoparticle density (~700 μm^{-2}), which is in a good agreement with our reported value of 6 nm. All of these observations are consistent with the effect of trace oxygen in Si NW growth, in which oxygen can stabilize Au atoms, deterring their surface diffusion and minimizing the Ostwald ripening process accordingly.[27,29,37]

At the same time, it is also important to assess the influence of this catalyst engineering on the electrical properties of GaAs NWs. As depicted in Figure 3, GaAs NW-parallel-arrayed thin-film FETs are fabricated by contact printing, as reported previously.[32,38] Because GaAs NWs grown by the 6-nm-thick H_2-annealed Au film are too short for successful NW printing, we purposefully employ the longer NWs prepared by the 4-nm-thick H_2-annealed Au film in the device fabrication used here. It is obvious in Figure 3a that the long and uniform NWs prepared by the air-stabilized Au film can easily enable the fabrication of FET with high-density NWs (>2 NW/μm) in the device channel (middle SEM), while using the optimized printing condition, the NW density in the device channel would inevitably become significantly reduced (~1 NW/μm) for the case of the H_2-annealed Au film (bottom SEM). In fact, an optimized printing condition such as the suitable applied pressure is essential to assemble high-density and uniform NW parallel arrays onto the device substrate. Too low pressure would not be efficient to transfer or print the thick NWs onto

DOI: 10.1021/acsami.5b00666
ACS Appl. Mater. Interfaces 2015, 7, 5591–5597

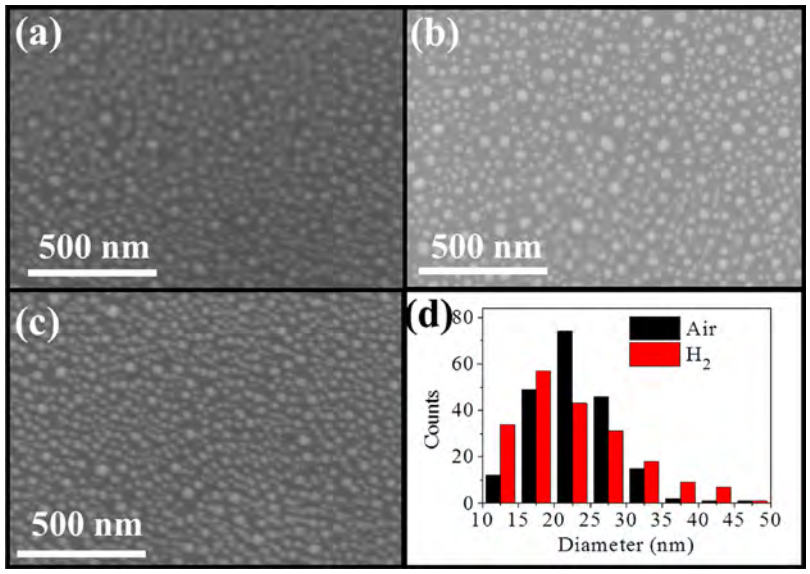

Figure 2. Comparison of the Au catalyst nanoparticles (6-nm-thick film) annealed in air and in H_2. (a and b) SEM images of Au nanoparticles annealed in H_2 for 10 and 60 min, respectively. (c) SEM image of Au nanoparticles annealed in air for 60 min. (d) Comparison of the Au diameter distribution annealed in air and in H_2 for 60 min.

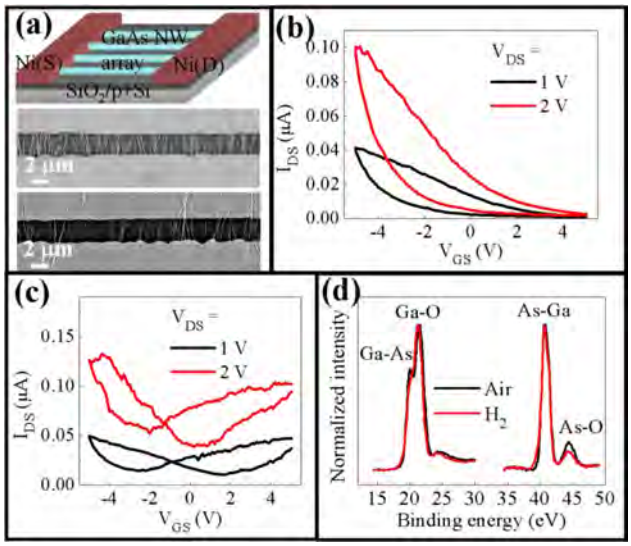

Figure 3. Electrical property comparison of GaAs NWs prepared by annealing Au catalyst films in air and in H_2. (a) Device schematic of the NW-arrayed FET and SEM images of the NW array assembled in the device channel (middle, NWs enabled by the air-stabilized catalyst; bottom, NWs made by the H_2-annealed catalyst). (b and c) $I_{DS}-V_{GS}$ curves of GaAs NW-arrayed FETs prepared by the Au film annealed in air (6 nm) and in H_2 (4 nm). (d) Normalized Ga 3d and As 3d XPS spectra of the NWs grown on the SiO_2/Si substrate.

foreign substrates in which the NWs are tightly anchored on the growth substrate; too high pressure would grind the thin NWs during the printing and mechanically damage the NW device channel. As a result, the long NWs (>10 μm) with uniform diameters achieved by the air-stabilized catalyst film can facilitate the assembly of high-density NW parallel arrays for large-scale device fabrication.

More importantly, the NW-arrayed FET using GaAs NWs grown by the air-stabilized Au film exhibits the reliable p-type characteristic, as shown in Figure 3b, while that made by the H_2-annealed Au film yields the ambipolar characteristic in Figure 3c (with the corresponding output characteristics given in Figure S4 in the SI). This ambipolar behavior is in good agreement with our previous results, in which the NWs prepared by H_2-annealed Au films would give p-type conductivity with NW diameter of less than 40 nm, ambipolar behavior in the diameter range of 40−70 nm, and the n-type characteristic for diameter of over 70 nm because of the acceptor-like defect states located between the intrinsic NW core and its amorphous native oxide shell.[20] However, because of the existence of trace oxygen in the material system (i.e., probably in the air-stabilized Au film), thicker oxide layers might exist in GaAs NWs and thus more electrons would be trapped from the NW core, resulting in pure p-type behavior. In this context, XPS analysis is employed to identify the composition of the surface layers on GaAs NWs, with Ga 3d and As 3d spectra shown in Figure 3d. It is clear that arsenic oxide has an increased relative intensity for the NWs prepared by air-stabilized Au films compared with those obtained by H_2-annealed films, suggesting that the increased surface oxide layer might contribute to the p-type conductivity here. All of these results are in accordance with the literature, in which surface-adsorbed oxygen or surface oxide layers are found to play an important role in modulating the electrical properties of semiconductor NWs,[39,40] especially for the effects of surface As−O bonds on GaAs.[41,42] Meanwhile, another probable contribution might come from the enhanced crystal quality of GaAs NWs grown with higher growth rate[18,43] and prepared by the air-stabilized Au film, as illustrated in the single-crystalline SAED pattern in Figure 1d in contrast with the previously reported defective NWs.[18] This reduced defect concentration would give fewer free electrons, and thus thicker surface electron depletion layers would be possible to yield the thick and p-type GaAs NWs.[5] Therefore, GaAs NWs grown by air-stabilized Au films explicitly indicate the advantages of improved p-type characteristics as well as better compatibility with contact printing for practical utilization.

In addition, the detailed NW growth processes and their corresponding effects on the NW electrical properties are also summarized schematically (Figure 4). Specifically, the Au

DOI: 10.1021/acsami.5b00666
ACS Appl. Mater. Interfaces 2015, 7, 5591−5597

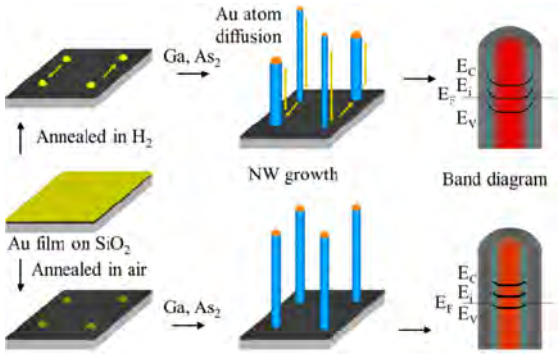

Figure 4. Illustrative schematics of the GaAs NW growth process utilizing Au catalytic nanoparticles annealed in H_2 and in air. The Au atoms existing in a H_2 atmosphere are surface-active and thus contribute to Ostwald ripening of nanoparticles during NW growth. Moreover, these nanoparticles would become stabilized in the air annealing and thus lead to uniform NW growth. At the same time, the oxygen residual existing in the air-annealing step would induce thicker surface oxide layers, contributing to the p-type conductivity, compared with the conventional ambipolar ones obtained by the H_2-annealed catalyst.

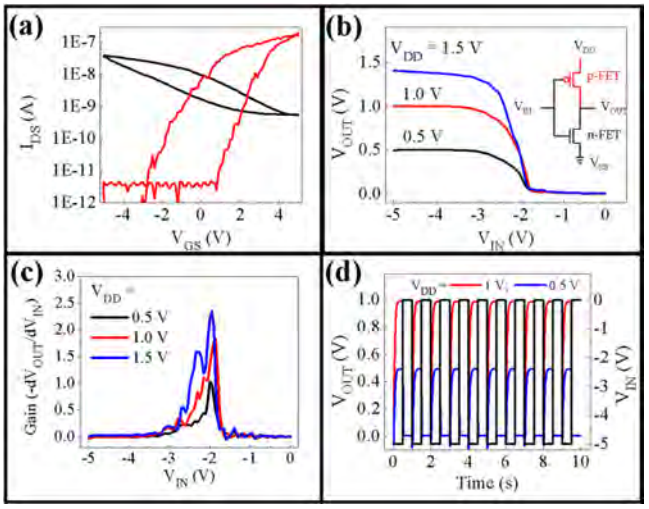

Figure 5. Electrical characteristics of fabricated NW CMOS inverters. (a) $I-V$ curves of the p- and n-type device components. (b) Voltage transformation curves and the CMOS circuit diagram (inset). (c) Gains of the inverter. (d) Transient response of the inverter.

catalyst film is first annealed into nanoparticles with active surfaces at a temperature of 800 °C for 10 min, in which the particles suffer from Ostwald ripening in the H_2 atmosphere and later yield the large NW diameter distribution in the subsequent growth process. In contrast, the Au nanoparticles are relatively more stable when annealed in air, which might be attributed to an oxygen effect similar to that reported in the literature;[27] as a result, the obtained NWs would have relatively uniform diameters. Moreover, this air-stabilization effect might as well contribute to thicker surface oxide layers of GaAs NWs, which would deplete more electrons from the NW core with possibly better crystal quality, moving the energy bands upward for the p-type conductivity. On the other hand, GaAs NWs prepared by H_2-annealed films would have the intrinsic band lying near the Fermi level, making the ambipolar conductivity of NWs in accordance with the previous reports.[5,20]

To further explore the potential electrical applications of these p-type GaAs NWs enabled by the air-stabilized Au catalyst film, the NW-arrayed FET is then integrated with an n-type InP NW FET[44] to form a CMOS inverter, as shown in Figure 5. Figure 5a gives the $I_{DS}-V_{GS}$ curves of the p- and n-type FETs, respectively, and Figure 5b illustrates the voltage transformation property of the inverter, with the circuit diagram detailed in the inset. It is clear that the inverter can effectively convert logic "1" (high input voltage) into logic "0" (low output voltage), and vice versa. It is also worth noting that the inverter can operate at a relatively low voltage (V_{DD}) of 0.5−1.5 V, together with the low leakage current, minimizing the power consumption.[5] Moreover, the gains can be kept high as well in the range of 1−2.5, as displayed in Figure 5c. The transient response to the alternate input voltage is also assessed (Figure 5d), in which the circuit is still operative at a working voltage as low as 0.5 V. Therefore, the CMOS inverter comprised of both p- and n-type NW devices can perform efficiently at both steady and transient conditions, indicating the reliability and versatility of these diameter and electrical property controls through engineering of the catalyst in NW growth. All of these would facilitate an important advancement of realizing NW building blocks for next-generation electronics.

CONCLUSIONS

In summary, simple annealing of the Au nanoparticles in air right before GaAs NW growth is an effective method to stabilize the Au catalytic particles in order to avoid Ostwald ripening, which can lead to more uniform diameter distribution, with the relative standard deviation (σ) of ∼20% employing the 4−12-nm-thick Au films. In comparison, conventional annealing of the Au catalyst film in H_2 would facilitate Au atom surface diffusion for Ostwald ripening, and thus the grown NWs would have the far larger diameter distribution ($\sigma \sim 20-60\%$). Importantly, the uniform diameter distribution can enable the uniform p-type conductivity of GaAs NWs and benefit high-density NW-arrayed FET fabrication. These p-type NW-arrayed FETs are then successfully integrated into CMOS inverters with n-type InP NW FETs, which can operate at low voltages of 0.5−1.5 V and perform effectively to both direct- and alternating-current inputs. All of these results explicitly demonstrate the promise of these NW morphology and electrical property modulations through the catalyst engineering for next-generation electronics.

ASSOCIATED CONTENT

Supporting Information

EDS spectrum taken on the NW catalyst tip, SEM image and NW diameter histogram of GaAs NWs prepared by vacuum annealing, SEM images and diameter histograms of GaAs NWs prepared by 4- and 12-nm Au catalyst films annealed in H_2 and air, and $I_{DS}-V_{DS}$ curves of printed NW-arrayed FETs. This material is available free of charge via the Internet at http://pubs.acs.org.

AUTHOR INFORMATION

Corresponding Author

*E-mail: johnnyho@cityu.edu.hk.

Author Contributions

§These authors contributed equally to this work.

Notes

The authors declare no competing financial interest.

DOI: 10.1021/acsami.5b00666
ACS Appl. Mater. Interfaces 2015, 7, 5591−5597

■ ACKNOWLEDGMENTS

This research is supported by the Early Career Scheme of the Research Grants Council of Hong Kong SAR, China (CityU 139413), the National Natural Science Foundation of China (Grants 51202205 and 51402160), the State Key Laboratory of Multiphase Complex Systems (MPCS-2014-C-01), and the Science Technology and Innovation Committee of Shenzhen Municipality (Grant JCYJ20140419115507588) and was supported by a grant from the Shenzhen Research Institute, City University of Hong Kong.

■ REFERENCES

(1) Gudiksen, M. S.; Lauhon, L. J.; Wang, J.; Smith, D. C.; Lieber, C. M. Growth of Nanowire Superlattice Structures for Nanoscale Photonics and Electronics. *Nature* **2002**, *415*, 617−620.

(2) Tomioka, K.; Yoshimura, M.; Fukui, T. A III−V Nanowire Channel on Silicon for High-Performance Vertical Transistors. *Nature* **2012**, *488*, 189−192.

(3) Takei, K.; Takahashi, T.; Ho, J. C.; Ko, H.; Gillies, A. G.; Leu, P. W.; Fearing, R. S.; Javey, A. Nanowire Active-Matrix Circuitry for Low-Voltage Macroscale Artificial Skin. *Nat. Mater.* **2010**, *9*, 821−826.

(4) Ford, A. C.; Ho, J. C.; Chueh, Y. L.; Tseng, Y. C.; Fan, Z. Y.; Guo, J.; Bokor, J.; Javey, A. Diameter-Dependent Electron Mobility of InAs Nanowires. *Nano Lett.* **2009**, *9*, 360−365.

(5) Han, N.; Hou, J. J.; Wang, F. Y.; Yip, S.; Yen, Y. T.; Yang, Z. X.; Dong, G. F.; Hung, T.; Chueh, Y. L.; Ho, J. C. GaAs Nanowires: From Manipulation of Defect Formation to Controllable Electronic Transport Properties. *ACS Nano* **2013**, *7*, 9138−9146.

(6) Yang, Z. X.; Han, N.; Wang, F. Y.; Cheung, H. Y.; Shi, X. L.; Yip, S.; Hung, T.; Lee, M. H.; Wong, C. Y.; Ho, J. C. Carbon Doping of InSb Nanowires for High-Performance p-Channel Field-Effect-Transistors. *Nanoscale* **2013**, *5*, 9671−9676.

(7) Yang, Z. X.; Han, N.; Fang, M.; Lin, H.; Cheung, H. Y.; Yip, S. P.; Wang, E. J.; Hung, T. F.; Wong, C. Y.; Ho, J. C. Surfactant-Assisted Chemical Vapour Deposition of High-Performance Small-Diameter GaSb Nanowires. *Nat. Commun.* **2014**, *5*,.

(8) Duan, X. F.; Lieber, C. M. General Synthesis of Compound Semiconductor Nanowires. *Adv. Mater.* **2000**, *12*, 298−302.

(9) Noborisaka, J.; Motohisa, J.; Hara, S.; Fukui, T. Fabrication and Characterization of Freestanding GaAs/AlGaAs Core−Shell Nanowires and Algaas Nanotubes by Using Selective-Area Metalorganic Vapor Phase Epitaxy. *Appl. Phys. Lett.* **2005**, *87*, 093109.

(10) Fortuna, S. A.; Li, X. L. GaAs MESFET with a High-Mobility Self-Assembled Planar Nanowire Channel. *IEEE Electron Device Lett.* **2009**, *30*, 593−595.

(11) del Alamo, J. A. Nanometre-Scale Electronics with III−V Compound Semiconductors. *Nature* **2011**, *479*, 317−323.

(12) Nah, J.; Fang, H.; Wang, C.; Takei, K.; Lee, M. H.; Plis, E.; Krishna, S.; Javey, A. III−V Complementary Metal−Oxide−Semiconductor Electronics on Silicon Substrates. *Nano Lett.* **2012**, *12*, 3592−3595.

(13) Wang, F.; Yip, S.; Han, N.; Fok, K.; Lin, H.; Hou, J. J.; Dong, G.; Hung, T.; Chan, K.; Ho, J. C. Surface Roughness Induced Electron Mobility Degradation in InAs Nanowires. *Nanotechnology* **2013**, *24*, 375202.

(14) Hou, J. J.; Wang, F. Y.; Han, N.; Zhu, H. S.; Fok, K.; Lam, W.; Yip, S.; Hung, T.; Lee, J. E. Y.; Ho, J. C. Diameter Dependence of Electron Mobility in InGaAs Nanowires. *Appl. Phys. Lett.* **2013**, *102*, 093112.

(15) Zhang, G. Q.; Tateno, K.; Sanada, H.; Tawara, T.; Gotoh, H.; Nakano, H. Synthesis of GaAs Nanowires with Very Small Diameters and Their Optical Properties with the Radial Quantum-Confinement Effect. *Appl. Phys. Lett.* **2009**, *95*, 123104.

(16) Duan, X.; Wang, J.; Lieber, C. Synthesis and Optical Properties of Gallium Arsenide Nanowires. *Appl. Phys. Lett.* **2000**, *76*, 1116.

(17) Johansson, J.; Dick, K.; Caroff, P.; Messing, M.; Bolinsson, J.; Deppert, K.; Samuelson, L. Diameter Dependence of the Wurtzite−Zinc Blende Transition in InAs Nanowires. *J. Phys. Chem. C* **2010**, *114*, 3837−3842.

(18) Han, N.; Wang, F.; Hou, J. J.; Yip, S.; Lin, H.; Fang, M.; Xiu, F.; Shi, X.; Hung, T.; Ho, J. C. Manipulated Growth of GaAs Nanowires: Controllable Crystal Quality and Growth Orientations Via a Supersaturation-Controlled Engineering Process. *Cryst. Growth Des.* **2012**, *12*, 6243−6249.

(19) Schmidt, V.; Senz, S.; Gösele, U. Diameter-Dependent Growth Direction of Epitaxial Silicon Nanowires. *Nano Lett.* **2005**, *5*, 931−935.

(20) Han, N.; Wang, F.; Hou, J. J.; Xiu, F.; Yip, S.; Hui, A. T.; Hung, T.; Ho, J. C. Controllable P−N Switching Behaviors of GaAs Nanowires via an Interface Effect. *ACS Nano* **2012**, *6*, 4428−4433.

(21) Ford, A. C.; Ho, J. C.; Fan, Z. Y.; Ergen, O.; Altoe, V.; Aloni, S.; Razavi, H.; Javey, A. Synthesis, Contact Printing, and Device Characterization of Ni-Catalyzed, Crystalline InAs Nanowires. *Nano Res.* **2008**, *1*, 32−39.

(22) Wu, Z. H.; Mei, X. Y.; Kim, D.; Blumin, M.; Ruda, H. E. Growth of Au-Catalyzed Ordered GaAs Nanowire Arrays by Molecular-Beam Epitaxy. *Appl. Phys. Lett.* **2002**, *81*, 5177−5179.

(23) Han, N.; Hou, J. J.; Wang, F.; Yip, S.; Lin, H.; Fang, M.; Xiu, F.; Shi, X.; Hung, T.; Ho, J. C. Large-Scale and Uniform Preparation of Pure-Phase Wurtzite GaAs NWs on Non-Crystalline Substrates. *Nanoscale Res. Lett.* **2012**, *7*, 1−6.

(24) Mantzaris, N. V. Liquid-Phase Synthesis of Nanoparticles: Particle Size Distribution Dynamics and Control. *Chem. Eng. Sci.* **2005**, *60*, 4749−4770.

(25) Bastus, N. G.; Comenge, J.; Puntes, V. Kinetically Controlled Seeded Growth Synthesis of Citrate-Stabilized Gold Nanoparticles of up to 200 nm: Size Focusing Versus Ostwald Ripening. *Langmuir* **2011**, *27*, 11098−11105.

(26) Dai, X.; Dayeh, S. A.; Veeramuthu, V.; Larrue, A.; Wang, J.; Su, H. B.; Soci, C. Tailoring the Vapor−Liquid−Solid Growth toward the Self-Assembly of GaAs Nanowire Junctions. *Nano Lett.* **2011**, *11*, 4947−4952.

(27) Kodambaka, S.; Hannon, J. B.; Tromp, R. M.; Ross, F. M. Control of Si Nanowire Growth by Oxygen. *Nano Lett.* **2006**, *6*, 1292−1296.

(28) Kawashima, T.; Mizutani, T.; Nakagawa, T.; Torii, H.; Saitoh, T.; Komori, K.; Fujii, M. Control of Surface Migration of Gold Particles on Si Nanowires. *Nano Lett.* **2008**, *8*, 362−368.

(29) Hannon, J. B.; Kodambaka, S.; Ross, F. M.; Tromp, R. M. The Influence of the Surface Migration of Gold on the Growth of Silicon Nanowires. *Nature* **2006**, *440*, 69−71.

(30) Renard, V. T.; Jublot, M.; Gergaud, P.; Cherns, P.; Rouchon, D.; Chabli, A.; Jousseaume, V. Catalyst Preparation for CMOS-Compatible Silicon Nanowire Synthesis. *Nat. Nanotechnol.* **2009**, *4*, 654−657.

(31) Han, N.; Wang, F. Y.; Hui, A. T.; Hou, J. J.; Shan, G. C.; Xiu, F.; Hung, T. F.; Ho, J. C. Facile Synthesis and Growth Mechanism of Ni-Catalyzed GaAs Nanowires on Non-Crystalline Substrates. *Nanotechnology* **2011**, *22*, 285607.

(32) Fan, Z. Y.; Ho, J. C.; Takahashi, T.; Yerushalmi, R.; Takei, K.; Ford, A. C.; Chueh, Y. L.; Javey, A. Toward the Development of Printable Nanowire Electronics and Sensors. *Adv. Mater.* **2009**, *21*, 3730−3743.

(33) Wacaser, B. A.; Dick, K. A.; Johansson, J.; Borgstrom, M. T.; Deppert, K.; Samuelson, L. Preferential Interface Nucleation: An Expansion of the VLS Growth Mechanism for Nanowires. *Adv. Mater.* **2009**, *21*, 153−165.

(34) Lee, S. T.; Zhang, Y. F.; Wang, N.; Tang, Y. H.; Bello, I.; Lee, C. S.; Chung, Y. W. Semiconductor Nanowires from Oxides. *J. Mater. Res.* **1999**, *14*, 4503−4507.

(35) Shi, W. S.; Zheng, Y. F.; Wang, N.; Lee, C. S.; Lee, S. T. A General Synthetic Route to III−V Compound Semiconductor Nanowires. *Adv. Mater.* **2001**, *13*, 591−594.

(36) Tsai, H. C.; Hu, E.; Perng, K.; Chen, M. K.; Wu, J. C.; Chang, Y. S. Instability of Gold Oxide Au_2O_3. *Surf. Sci.* **2003**, *537*, L447−L450.

DOI: 10.1021/acsami.5b00666
ACS Appl. Mater. Interfaces 2015, 7, 5591−5597

(37) Campbell, C. T.; Parker, S. C.; Starr, D. E. The Effect of Size-Dependent Nanoparticle Energetics on Catalyst Sintering. *Science* **2002**, *298*, 811−814.
(38) Han, N.; Wang, F. Y.; Hou, J. J.; Yip, S. P.; Lin, H.; Xiu, F.; Fang, M.; Yang, Z. X.; Shi, X. L.; Dong, G. F.; Hung, T. F.; Ho, J. C. Tunable Electronic Transport Properties of Metal−Cluster-Decorated III−V Nanowire Transistors. *Adv. Mater.* **2013**, *25*, 4445−4451.
(39) Kim, D. K.; Lai, Y. M.; Vemulkar, T. R.; Kagan, C. R. Flexible, Low-Voltage, and Low-Hysteresis PbSe Nanowire Field-Effect Transistors. *ACS Nano* **2011**, *5*, 10074−10083.
(40) He, R. R.; Yang, P. D. Giant Piezoresistance Effect in Silicon Nanowires. *Nat. Nanotechnol.* **2006**, *1*, 42−46.
(41) Huang, M.; Chang, Y.; Chang, C.; Lee, Y.; Chang, P.; Kwo, J.; Wu, T.; Hong, M. Surface Passivation of III−V Compound Semiconductors Using Atomic-Layer-Deposition-Grown Al_2O_3. *Appl. Phys. Lett.* **2005**, *87*, 252104.
(42) Sandroff, C. J.; Hegde, M. S.; Farrow, L. A.; Chang, C. C.; Harbison, J. P. Electronic Passivation of GaAs-Surfaces through the Formation of Arsenic Sulfur Bonds. *Appl. Phys. Lett.* **1989**, *54*, 362−364.
(43) Joyce, H. J.; Gao, Q.; Tan, H. H.; Jagadish, C.; Kim, Y.; Fickenscher, M. A.; Perera, S.; Hoang, T. B.; Smith, L. M.; Jackson, H. E.; Yarrison-Rice, J. M.; Zhang, X.; Zou, J. Unexpected Benefits of Rapid Growth Rate for III−V Nanowires. *Nano Lett.* **2009**, *9*, 695−701.
(44) Hui, A. T.; Wang, F.; Han, N.; Yip, S. P.; Xiu, F.; Hou, J. J.; Yen, Y. T.; Hung, T. F.; Chueh, Y. L.; Ho, J. C. High-Performance Indium Phosphide Nanowires Synthesized on Amorphous Substrates: From Formation Mechanism to Optical and Electrical Transport Measurements. *J. Mater. Chem.* **2012**, *22*, 10704−10708.

DOI: 10.1021/acsami.5b00666
ACS Appl. Mater. Interfaces 2015, 7, 5591−5597